catalysts

MDPI

*Article*

# Synthesis of Durian-like $TiO_2$@CdS Core-Shell Structure and Study on $H_2$ Generation Properties

**Dongping Li [1,2,*], Zeheng Chen [1,2], Xin Wang [1,2,*], Zhenhong Zhong [1,2], Chunjun Chen [3] and Mengling Wu [4]**

1 The School of Material Science & Chemical Engineering, Harbin University of Science & Technology, Harbin 150040, China
2 Heilongjiang Provincial Key Laboratory of CO2 Resource Utilization and Energy Catalytic Materials, Harbin 150040, China
3 Institute of Chemistry, Chinese Academy of Sciences, Beijing 100190, China
4 School of Materials Science and Engineering, Nanjing Institute of Technology, Nanjing 211167, China
* Correspondence: huagong0003@163.com (D.L.); wangxin0120@163.com (X.W.)

**Abstract:** Novel durian-like $TiO_2$@CdS core-shell particles were synthesized through a solvothermal method in ethylenediamine solution and the obtained nanocomposites were characterized by scanning electron microscopy (SEM), powder X-ray diffraction (XRD), and transmission electron microscopic (TEM) techniques. It can be seen from the characterization that the synthesized core-shell structured particles show uniform size. The possible formation mechanism of $TiO_2$@CdS core-shell particles is also presented schematically. CdS grows on the $TiO_2$ surface in the form of nanorods, turning the $TiO_2$@CdS composite particles into durian-like structures. The durian-like $TiO_2$@CdS core-shell particles prepared in the experiment can overcome the disadvantages of $TiO_2$ and CdS, respectively. They not only produce a higher yield of $H_2$ than pure $TiO_2$; the durian-like $TiO_2$@CdS nanostructures formed at 180 °C for 16 h produced 2.5 times as much $H_2$ as did $TiO_2$, also showing enhanced stability as compared with pure CdS.

**Keywords:** $TiO_2$; CdS nanorods; core-shell structure; $H_2$ generation



**Citation:** Li, D.; Chen, Z.; Wang, X.; Zhong, Z.; Chen, C.; Wu, M. Synthesis of Durian-like $TiO_2$@CdS Core-Shell Structure and Study on $H_2$ Generation Properties. *Catalysts* **2022**, *12*, 1211. https://doi.org/10.3390/catal12101211

Academic Editors: Hongxing Dai, Xiang Wang, Yujun Zhu, Haibao Huang and Yunkun Zhao

Received: 25 August 2022
Accepted: 30 September 2022
Published: 11 October 2022



## 1. Introduction

In recent years, photocatalysis via titanium dioxide ($TiO_2$) has been widely investigated as a promising method for environmental and energy applications [1–3], and functional properties have been extensively used in various fields including photocatalytic degradation of pollutants [4–6], photocatalytic $CO_2$ reduction into energy fuels, water splitting, supercapacitors and lithium-ion batteries [7–10]. However, due to its broad band gap of 3.2 eV, $TiO_2$ is only sensitive to the light of wavelengths below 380 nm belonging to the UV range, which covers only 5% of the entire solar spectrum [11]. This draw back dramatically limits its conversion efficiency in solar applications. Recent research has focused on improving the photocatalytic efficiency of $TiO_2$ through a variety of material engineering approaches, such as improving charge electroactive surface area [12], utilization of co-catalyst immobilization, controlled faceting, and enhancing the visible-light activity of $TiO_2$ through doping [13–17]. Irfan et al., successfully utilized CoSe as a cocatalyst and ZnSe as a visible-light active semiconductor to significantly enhance the photocatalytic hydrogen production on ZnSe/CdS under visible light irradiation for inexpensive conversion of solar energy to $H_2$ [18]. Pan et al., have successfully developed a hybrid photocatalytic system consisting of CdS NSs as PS and free-standing $Fe_2P$ NPs as cocatalysts for photocatalytic hydrogen production from water under visible light [19]. According to previous reports, the charge can be separated efficiently at the heterointerface, thus suitable design of the heterointerface between the other semiconductor catalysts and $TiO_2$ will be an effective strategy for enhancing the performance of photocatalysis [20,21].

Cadmium sulfide (CdS) which is an important II–VI semiconductor ($E\hat{g}$ = 2.42 eV (515 nm) at room temperature) with many excellent physical and chemical properties [22], has been used as a light-harvesting sensitizer to improve the photoelectric properties of $TiO_2$ because of its appropriate direct energy band gap. Recently, $TiO_2$/CdS composite materials have attracted great interest. They could compensate the disadvantages of the individual components based on some synergistic effects, such as efficient charge separation and migration, expanded visible light response, and improved photostability [23–25]. Cao et al., prepared $TiO_2$/CdS core-shell nanorod arrays with visible light activity by a two-step method. Thish increased the probability of electron–hole separation and extended the range of the $TiO_2$ photoresponse from ultraviolet to visible regions [26].

Many fundamental properties of semiconductor materials are dependent on the size and shape of their particles. Controlling the relevant size and shape would provide opportunities for tailoring properties of materials and offer possibilities for observing attractive and useful physical phenomena [27]. Therefore, materials engineering in nanometer-scale has attracted much attention in optics, electronics, magnetics, catalysis, and ceramics [28–32]. In this paper, $TiO_2$@CdS core-shell particles, with CdS nanorods as shell layers and $TiO_2$ nanoparticles as the corresponding core units, were successfully fabricated, in order to overcome the disadvantages of both $TiO_2$ and CdS, thus gaining better optical and electric performances. To the best of our knowledge, this is the first report on $TiO_2$@CdS core-shell particles with a durian-like surface structure.

## 2. Results and Discussion

### *2.1. SEM and TEM Characterizations*

SEM and TEM techniques were employed to characterize the morphology of the $TiO_2$@CdS particles obtained with different reaction times. As shown in Figure 1a, the commercially available $TiO_2$ nanoparticles with diameters of about 100 nm have a smooth surface. After adding a $CdCl_2$ solution, $SC(NH_2)_2$, $H_2NCH_2CH_2NH_2$ and conducting continuous heating for 8 h, we find the surface of $TiO_2$ is no longer smooth due to the formation of a $TiO_2$@CdS composite (Figure 1b). With an extended heating time (16 h), we observe the formation of durian-like $TiO_2$@CdS particles (Figure 1c) with various nanorods on the $TiO_2$ surface, with a diameter of 50 nm. We further used TEM to characterize the $TiO_2$@CdS particles. As shown in Figure 1d, the clear contrast between the core and the shell indeed proves that the CdS nanorods coat the surface of the $TiO_2$ nanoparticles. Furthermore, as shown in Figure 2 and Table 1, the ratio of S:Cd is ca. 1:1. The results of EDX basically indicate that the surface rods are CdS.

**Table 1.** The EDX data of Weight % and Atomic % of S and K Element in the sample.

| Element | Weight % | Atomic % |
|---|---|---|
| S K | 23.25 | 51.50 |
| Cd L | 76.75 | 48.50 |
| Totals | 100.00 | 100.00 |

Based on the above observations, we can conclude that the reaction time played a crucial role in controlling the durian-like morphology of the $TiO_2$@CdS. With the help of ethylenediamine, the CdS grows into a rod-like structure on the surface of the $TiO_2$ particles forming durian-like $TiO_2$@CdS particles (Figure 1c), as further confirmed by TEM (Figure 1d).

### *2.2. XRD Characterization*

The powder XRD patterns of the $TiO_2$, $TiO_2$@CdS and CdS samples prepared with different reaction times are shown in Figure 3. A typical diffraction peak located at $2\theta = 25.3^\circ$ is attributed to the (101) crystal planes of the anatase-phase $TiO_2$ (JCPDS no. 21-1272). The peaks at 26.5° and 28.2°observed in the XRD of $TiO_2$@CdS and CdS particles are attributed to (002) and (101) crystal planes of hexagonal CdS. If the reaction time lasts longer, the

(002) diffraction peak of the $TiO_2$@CdS samples becomes both stronger and narrower, as shown in Figure 3 ($TiO_2$@CdS, 16 h). The unusual (002) diffraction peak indicates that the sample ($TiO_2$@CdS, 16 h) is preferentially orientated along the c axis. The rod shape is confirmed by SEM and TEM photographs. In addition, the typical diffraction peak located at $2\theta = 25.3^\circ$ of anatase-phase $TiO_2$ is weak which can be explained by the thick coating of CdS on the surface of $TiO_2$. This result is also verified by the TEM photograph.

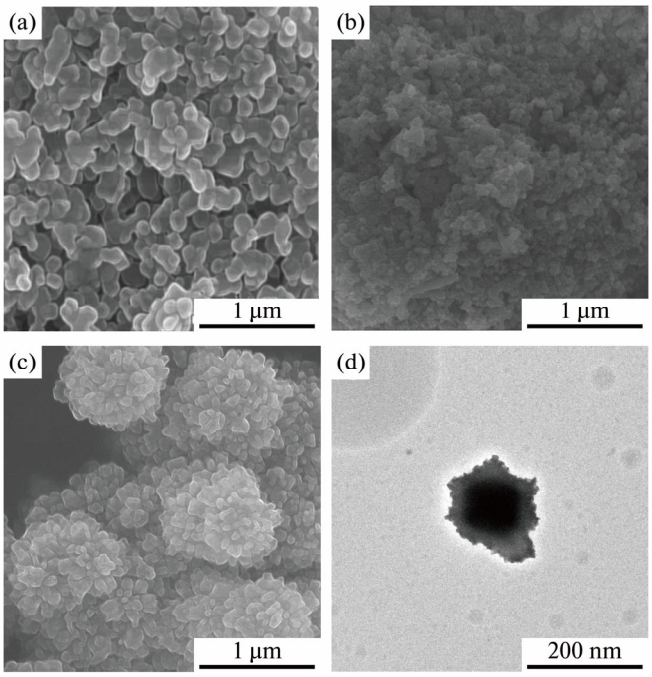


**Figure 1.** SEM and TEM image. (**a**) SEM image of $TiO_2$; (**b**) SEM image of $TiO_2$@CdS formed at 180 °C for 8 h; (**c**) SEM image of durian-like $TiO_2$@CdS nanostructure formed at 180 °C for 16 h; (**d**) TEM image of a durian-like $TiO_2$@CdS core-shell nanostructure formed at 180 °C for 16 h.

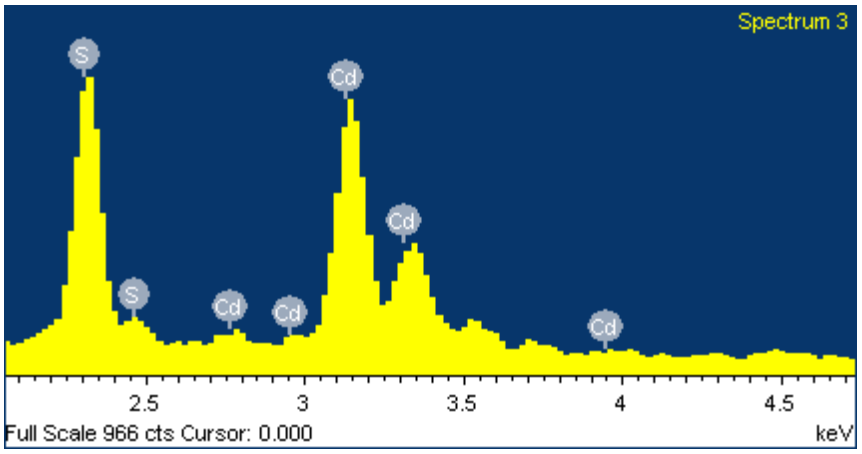


**Figure 2.** The EDX data of Weight % and Atomic % of S and Cd elements in the sample.

### *2.3. The Formation Mechanism of $TiO_2$@CdS Core-Shell Particles*

The possible formation mechanism of $TiO_2$@CdS core-shell particles is depicted schematically in Figure 4. The first step is to link the $Cd^{2+}$ to the $TiO_2$ surface through inorganic grafting which is achieved by impregnating $TiO_2$ nanoparticles in a $CdCl_2$ solution. In the second step, the addition of $SC(NH_2)_2$ promotes generation of CdS on the surface of the $TiO_2$ nanoparticle, which is used as the seed. In the third step, CdS grows in the

form of nanorods on the surface of $TiO_2$ with the help of ethylenediamine, which turns the composite particle into a durian-like structure.

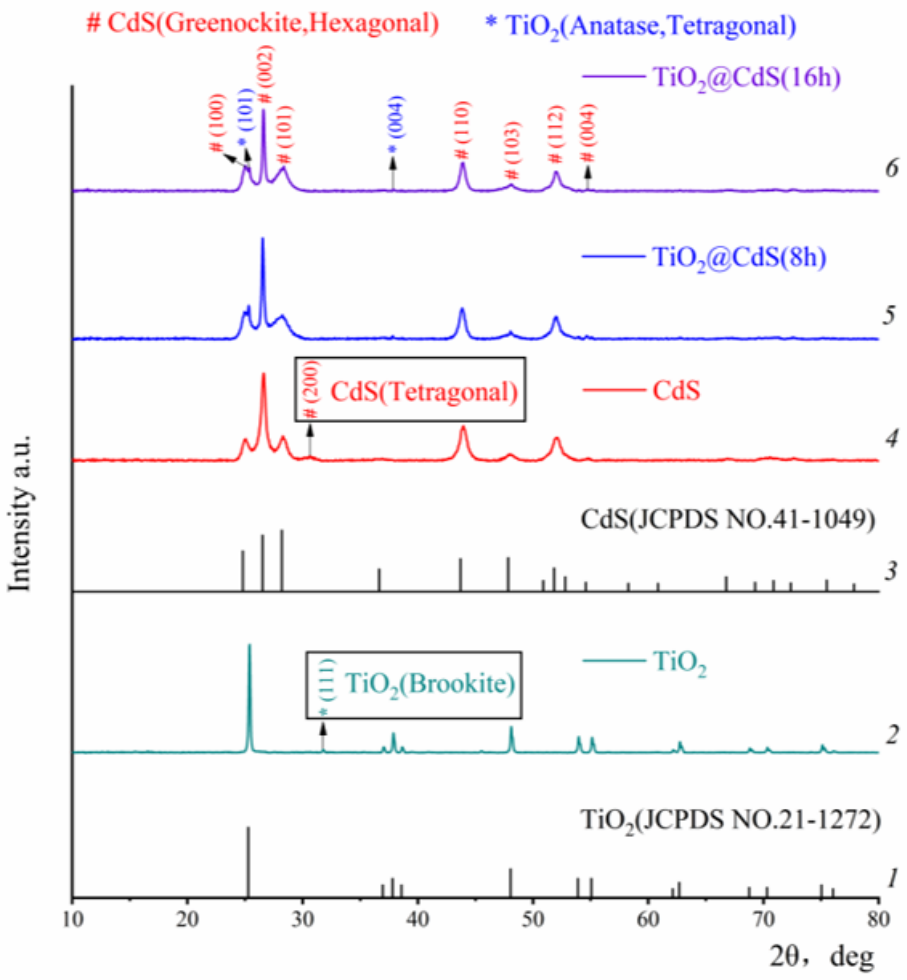


**Figure 3.** XRD patterns of the anatase-phase $TiO_2$ and $TiO_2$@CdS particles.

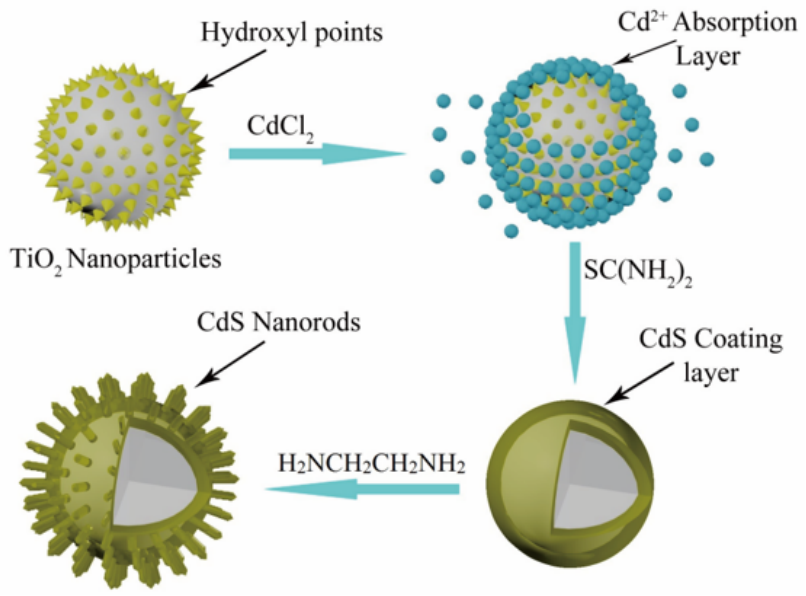


**Figure 4.** Schematic process for durian-like $TiO_2$@CdS core-shell structure.

### *2.4. Photocatalytic Reaction for $H_2$ Generation*

In order to verify the photocatalyst activity of the $TiO_2$@CdS particles, the photocatalytic hydrogen evolution ability under light irradiation was studied, and the results are shown in Table 2. We find that the efficiency of $H_2$ generation in the produced hybrid materials increases in the order $TiO_2$ < $TiO_2$@CdS (8 h) < durian-like $TiO_2$@CdS (16 h) with a maximum $H_2$ generation rate of 1065 μmol·$h^{-1}$·$g^{-1}$ for the durian-like $TiO_2$@CdS core/shell particles (16 h). This is two times larger than the activity of bare $TiO_2$ particles. The yield of $H_2$ of durian-like $TiO_2$@CdS (16 h) is higher than that of $TiO_2$@CdS (8 h). The results indicate that the durian-like $TiO_2$@CdS particles have better photocatalytic activity than $TiO_2$ particles since the CdS nanorod can expand the visible light response and improve charge separation and migration. The yield of $H_2$ of pure CdS is higher than that of durian-like $TiO_2$@CdS (16 h), but pure CdS is less stable, as suggested by a color change from yellow to black. The color of the hybrid materials $TiO_2$@CdS is not changed during the photocatalytic reaction.

**Table 2.** $H_2$ generation rate of different samples.

| Sample | $H_2$ Generation Rate, μmol·$h^{-1}$·$g^{-1}$ |
|---|---|
| $TiO_2$ | 400 |
| $TiO_2$@CdS (8 h) | 588 |
| $TiO_2$@CdS (16 h) | 1065 |
| CdS | 3550 |

Additionally, the reproducibility experiments have been performed. The $H_2$ generation rate of durian-like $TiO_2$@CdS (16 h) decreased to 800 μmol·$h^{-1}$·$g^{-1}$ after four cycle reaction (see the Figure 5). In contrast, the $H_2$ generation rate of pure CdS dropped to 400 μmol·$h^{-1}$·$g^{-1}$ in the second cycle reaction. Meanwhile, the SEM experiments of both CdS and durian-like $TiO_2$@CdS after photocatalytic reaction have also been performed (Figure 6). The results indicated that the particle size of durian-like $TiO_2$@CdS slightly changed as compared with the pure CdS. In addition, no obvious change was observed before and after catalysis in the XRD of the $TiO_2$@CdS (Figure 6e). Thus, the reproducibility of $H_2$ generation rate of durian-like $TiO_2$@CdS is basically good. Compared with the state-of-the-art catalysts, the activity and stability of $TiO_2$@CdS is comparable.

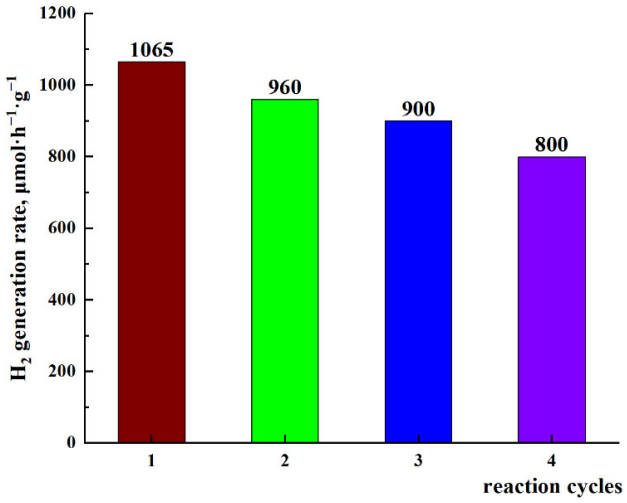


**Figure 5.** The diagram of $H_2$ generation rate of $TiO_2$@CdS four cycle reaction.

From the above results, we can observe that the activity of $H_2$ generation over $TiO_2$@CdS was higher than that of the $TiO_2$, and the stability of $TiO_2$@CdS was better than that of CdS. Thus, we can assume that the charged species can be separated over the

composites, and photocorrosion is severely inhibited. Hence, we can assume that a typical Z-scheme mechanism was occurring over the $TiO_2$@CdS. Under simulated sunlight illumination, both $TiO_2$ and CdS can be excited to produce photoinduced electrons and holes. The photoinduced electrons in CdS tend to keep in the CB of CdS, and the photoinduced holes in $TiO_2$ remain in the VB of $TiO_2$. Meanwhile, the photoinduced electrons in the CB of $TiO_2$ combine with the photoinduced holes in VB of CdS (Figure 6f). Thus, the holes over the CdS can be reduced, and the photooxidation reaction may occur on the surface of $TiO_2$ rather than the CdS. Therefore, the carriers can be separated and photocorrosion can be inhibited. In addition, the photo-current responses of CdS, $TiO_2$@CdS and $TiO_2$ were tested to gain a deeper understanding of the efficacy of photoexcited charge separation. As shown in Figure 6g, we can observe that the photocurrent intensity of $TiO_2$@CdS (16) was higher than that of $TiO_2$, indicating more effective charge separation in $TiO_2$@CdS (16). Although the CdS exhibited the highest photocurrent, the $H_2$ generation rate of pure CdS dropped seriously.

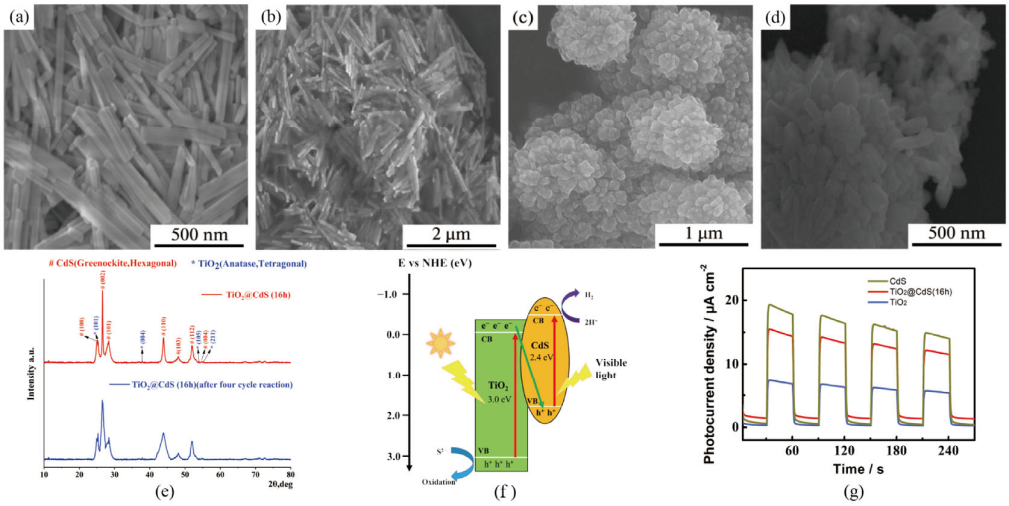


**Figure 6.** (**a**) SEM image of pure CdS, (**b**) SEM image of pure CdS after reaction, (**c**) SEM image of $TiO_2$@CdS, (**d**) SEM image of $TiO_2$@CdS after reaction, (**e**) XRD patterns of $TiO_2$@CdS before and after the reaction, (**f**) Illustration of the photocatalytic mechanism, (**g**) The photocurrent measurements over $TiO_2$, CdS and $TiO_2$@CdS (16 h).

## 3. Materials and Methods

### *3.1. Subsection*

All chemicals were commercially purchased and used without purification. The source of reagents that we used: $TiO_2$ (Tianjin No.3 Chemical Reagent Factory, Tianjin, China), $CdCl_2$ (Tianjin GuangFu Science and Technology Development Co., Ltd., Tianjin, China), thiourea (Tianjin Zhiyuan Chemical Reagent Co., Ltd., Tianjin, China), ethylenediamine (Tianjin Zhiyuan Chemical Reagent Co., Ltd., Tianjin, China) and Ethanol (Tianjin TianLi Chemical Co., Ltd., Tianjin, China).

### *3.2. Preparation of $TiO_2$@CdS Core-Shell Particles*

These particles were synthesized by a solvothermal method [33,34]. The commercial anatase-phase $TiO_2$ nanoparticles (1 g, 0.013 mol) were added to dilute nitric acid (10 mL, 1 mol·$L^{-1}$) with ultrasound for 4 h, and were collected and washed with distilled water to neutral. The final products were dried at 80 °C for 4 h in a vacuum box. The obtained $TiO_2$ (0.1 g) nanoparticles and 5 mL of an aqueous solution of $CdCl_2$ (1 mol·$L^{-1}$) were added to a beaker with a capacity of 100 mL and were stirred magnetically for 4 h at room temperature. 5 mL of a thiourea solution (1.5 mol·$L^{-1}$) and the mixture described above were added to a teflon-lined stainless steel autoclave with a 25 mL capacity. The autoclave was filled with 10 mL ethylenediamine solution up to about 80% of the total volume. The solution was

stirred and treated with ultra-sound. The autoclave was maintained at 180 °C for 8–16 h and then allowed to cool to room temperature. Yellow precipitates were collected and washed with ethanol and distilled water to remove residues of organic material. The final products were dried at 80 °C for 4 h in a vacuum box. The pure CdS was prepared by the same method without $TiO_2$.

### *3.3. Characterization of $TiO_2$@CdS Core-Shell Particles*

The morphologies of the $TiO_2$ nanoparticles and durian-like $TiO_2$@CdS core-shell particles were characterized by scanning electron microscopy (SEM, SU8020) and transmission electron microscopy (TEM, JEM-2100). To facilitate the investigation of the detailed surface morphology of $TiO_2$@CdS, no conductive metal layer such as Au, Pd/Au, Cr, or carbon layer was coated on the sample surface. The samples were further analyzed with a Bruker D8 Avance X-ray diffractometer (XRD) using Ni-filtered Cu Kα radiation at 40 kV and 40 mA in the 2θ range of 20–80°, with a scan rate of 0.02° per second.

### *3.4. Photocatalytic Experiment*

Photocatalytic reactions of hydrogen production by water splitting were conducted in a gas-closed system with a side irradiation Pyrex cell. An aluminum alloy shell was employed outside the Pyrex cell to reflect and gather the visible light originating from Xe lamp. A water cycling system was used to maintain the reaction temperature.

Photocatalyst powder (10 mg) was dispersed in a solution (2 mL) containing 0.35 mol·$L^{-1}$ $Na_2S$ and 0.25 mol·$L^{-1}$$Na_2SO_3$. After being evacuated and flushed by $N_2$ gas for over 10 min, the photocatalysts were irradiated by visible light ($\lambda \geq 300$ nm) from a 300 W Xe lamp for 4 h. The amount of $H_2$ gas was determined using a gas chromatograph (Bruker GC-4890, using column type TDX01).

## 4. Conclusions

In summary, novel durian-like $TiO_2$@CdS core-shell particles were synthesized through a solvothermal method in ethylenediamine solution. As demonstrated, CdS coated the surface of the $TiO_2$ material. The reaction time plays a crucial role in controlling the nucleation and growth of crystallites; with a prolonged reaction time, CdS gradually forms a rod shape, which effectively enhances visible light absorption and possesses a high electron affinity. The durian-shaped $TiO_2$@CdS composite not only produced a higher yield of $H_2$ than pure $TiO_2$, but also possessed an enhanced stability as compared with the pure CdS. Therefore, the durian-like $TiO_2$@CdS core-shell particles might be a good catalyst for application in photocatalysis.

**Author Contributions:** Conceptualization, Z.C. and D.L.; methodology, Z.C. and X.W.; software, C.C.; investigation, D.L. and Z.Z.; data curation, X.W.; writing—original draft preparation, Z.C.; writing—review and editing, D.L., Z.C., X.W., Z.Z., C.C. and M.W. All authors have read and agreed to the published version of the manuscript.

**Funding:** This research received no external funding.

**Data Availability Statement:** Not applicable.

**Acknowledgments:** The authors thank the Harbin University of Science & Technology and Chinese Academy of Sciences for experimental and technical support.

**Conflicts of Interest:** The authors declare no conflict of interest.

## References

1. Ge, M.; Cao, C.; Huang, J.; Li, S.; Chen, Z.; Zhang, K.-Q.; Al-Deyab, S.S.; Lai, Y. A review of one-dimensional $TiO_2$ nanostructured materials for environmental and energy applications. *J. Mater. Chem. A* **2016**, *4*, 6772–6801. [CrossRef]
2. Pelaez, M.; Nolan, N.T.; Pillai, S.C.; Seery, M.K.; Falaras, P.; Kontos, A.G.; Dunlop, P.S.M.; Hamilton, J.W.J.; Byrne, J.A.; O'Shea, K. A review on the visible light active titanium dioxide photocatalysts for environmental applications. *Appl. Catal. B Environ.* **2012**, *125*, 331–349. [CrossRef]

3. Rempel, A.A.; Valeeva, A.A.; Vokhmintsev, A.S.; Weinstein, I.A. Titanium dioxide nanotubes: Synthesis, structure, properties and applications. *Russ. Chem. Rev.* **2021**, *90*, 1397–1414. [CrossRef]
4. Falletta, E.; Bianchi, C.L.; Morazzoni, F.; Polissi, A.; Di Vincenzo, F.; Bellobono, I.R. Tungsten Trioxide and Its $TiO_2$ Mixed Composites for the Photocatalytic Degradation of NOX and Bacteria (*Escherichia coli*) Inactivation. *Catalysts* **2022**, *12*, 822. [CrossRef]
5. Bergamonti, L.; Graiff, C.; Bergonzi, C.; Potenza, M.; Reverberi, C.; Ossiprandi, M.C.; Lottici, P.P.; Bettini, R.; Elviri, L. Photodegradation of Pharmaceutical Pollutants: New Photocatalytic Systems Based on 3D Printed Scaffold-Supported Ag/$TiO_2$ Nanocomposite. *Catalysts* **2022**, *12*, 580. [CrossRef]
6. Yu, J.; Caravaca, A.; Guillard, C.; Vernoux, P.; Zhou, L.; Wang, L.; Lei, J.; Zhang, J.; Liu, Y. Carbon Nitride Quantum Dots Modified $TiO_2$ Inverse Opal Photonic Crystal for Solving Indoor VOCs Pollution. *Catalysts* **2021**, *11*, 464. [CrossRef]
7. Xiao, T.; Chen, Y.; Liang, Y. Ni(II) Tetra(4-carboxylphenyl)porphyrin-Sensitized $TiO_2$ Nanotube Array Composite for Efficient Photocatalytic Reduction of $CO_2$. *J. Phys. Chem. C* **2022**, *126*, 9742–9752. [CrossRef]
8. Liu, J.; Liu, B.; Ren, Y.; Yuan, Y.; Zhao, H.; Yang, H.; Liu, S. Hydrogenated nanotubes/nanowires assembled from $TiO_2$ nanoflakes with exposed {111} facets: Excellent photo-catalytic $CO_2$ reduction activity and charge separation mechanism between (111) and (111) polar surfaces. *J. Mater. Chem. A* **2019**, *7*, 14761–14775. [CrossRef]
9. Appadurai, T.; Subramaniyam, C.M.; Kuppusamy, R.; Karazhanov, S.; Subramanian, B. Electrochemical Performance of Nitrogen-Doped $TiO_2$ Nanotubes as Electrode Material for Supercapacitor and Li-Ion Battery. *Molecules* **2019**, *24*, 2952. [CrossRef]
10. Li, H.; Wang, S.; Wang, M.; Gao, Y.; Tang, J.; Zhao, S.; Chi, H.; Zhang, P.; Qu, J.; Fan, F.; et al. Enhancement of Plasmon-Induced Photoelectrocatalytic Water Oxidation over Au/$TiO_2$ with Lithium Intercalation. *Angew. Chem. Int. Ed.* **2022**, *61*, e202204272.
11. Nam, Y.; Lim, J.H.; Ko, K.C.; Lee, J.Y. Photocatalytic activity of $TiO_2$ nanoparticles: A theoretical aspect. *J. Mater. Chem. A* **2019**, *7*, 13833–13859. [CrossRef]
12. Al Qarni, F.; Alomair, N.A.; Mohamed, H.H. Environment-Friendly Nanoporous Titanium Dioxide with Enhanced Photocatalytic Activity. *Catalysts* **2019**, *9*, 799. [CrossRef]
13. Yang, B.; Ma, Z.; Wang, Q.; Yang, J. Synthesis and Photoelectrocatalytic Applications of $TiO_2$/ZnO/Diatomite Composites. *Catalysts* **2022**, *12*, 268. [CrossRef]
14. Cai, M.; Cao, S.; Zhuo, Z.; Wang, X.; Shi, K.; Cheng, Q.; Xue, Z.; Du, X.; Shen, C.; Liu, X.; et al. Fabrication of $Ni_2P$ Cocatalyzed CdS Nanorods with a Well-Defined Heterointerface for Enhanced Photocatalytic $H_2$ Evolution. *Catalysts* **2022**, *12*, 417. [CrossRef]
15. Gao, X.-F.; Sun, W.-T.; Hu, Z.-D.; Ai, G.; Zhang, Y.-L.; Feng, S.; Li, F.; Peng, L.-M. An Efficient Method To Form Heterojunction CdS/$TiO_2$ Photoelectrodes Using Highly Ordered $TiO_2$ Nanotube Array Films. *J. Phys. Chem. C* **2009**, *113*, 20481–20485. [CrossRef]
16. Kang, X.; Chaperman, L.; Galeckas, A.; Ammar, S.; Mammeri, F.; Norby, T.; Chatzitakis, A. Water Vapor Photoelectrolysis in a Solid-State Photoelectrochemical Cell with $TiO_2$ Nanotubes Loaded with CdS and CdSe Nanoparticles. *ACS Appl. Mater. Int.* **2021**, *13*, 46875–46885. [CrossRef]
17. Pal, S.; Taurino, A.; Catalano, M.; Licciulli, A. Block Copolymer and Cellulose Templated Mesoporous $TiO_2$-$SiO_2$ Nanocomposite as Superior Photocatalyst. *Catalysts* **2022**, *12*, 770. [CrossRef]
18. Irfan, R.M.; Tahir, M.H.; Maqsood, M.; Lin, Y.; Bashir, T.; Iqbal, S.; Zhao, J.; Gao, L.; Haroon, M. CoSe as non-noble-metal cocatalyst integrated with heterojunction photosensitizer for inexpensive $H_2$ production under visible light. *J. Catal.* **2020**, *390*, 196–205. [CrossRef]
19. Pan, Z.; Wang, R.; Li, J.; Iqbal, S.; Liu, W.; Zhou, K. $Fe_2P$ nanoparticles as highly efficient freestanding co-catalyst for photocatalytic hydrogen evolution. *Int. J. Hydrogen Energy* **2018**, *43*, 5337–5345. [CrossRef]
20. Kim, H.-I.; Kim, J.; Kim, W.; Choi, W. Enhanced Photocatalytic and Photoelectrochemical Activity in the Ternary Hybrid of CdS/$TiO_2$/$WO_3$ through the Cascadal Electron Transfer. *J. Phys. Chem. C* **2011**, *115*, 9797–9805. [CrossRef]
21. Lv, Z.; Wang, Y.; Liu, Y.; Wang, J.; Qin, G.; Guo, Z.; Zhang, C. NiB as a Substitute for the Pt Cocatalyst in CdS with Enhanced Visible-Light Photocatalytic $H_2$ Production. *J. Phys. Chem. C* **2022**, *126*, 9041–9050. [CrossRef]
22. Jie, J.S.; Zhang, W.J.; Jiang, Y.; Meng, X.M.; Li, Y.Q.; Lee, S.T. Photoconductive Characteristics of Single-Crystal CdS Nanoribbons. *Nano Lett.* **2006**, *6*, 1887–1892. [CrossRef] [PubMed]
23. Zhang, J.; Cai, P.; Lin, J. Modulation of the Band Bending of CdS by Fluorination to Facilitate Photoinduced Electron Transfer for Efficient $H_2$ Evolution over Pt/CdS. *J. Phys. Chem. C* **2022**, *126*, 7896–7902. [CrossRef]
24. Du, Y.-e.; Niu, X.; He, X.; Hou, K.; Liu, H.; Zhang, C. Synthesis and Photocatalytic Activity of $TiO_2$/CdS Nanocomposites with Co-Exposed Anatase Highly Reactive Facets. *Molecules* **2021**, *26*, 6031. [CrossRef] [PubMed]
25. Guo, N.; Wang, C.; Bao, W.; Zeng, Y.; Yu, H. Hollow $TiO_2$@CdS nanosphere: Interface construction for spatial charge separation and higher charge transfer efficiency. *J. Environ. Chem. Eng.* **2021**, *9*, 106211. [CrossRef]
26. Cao, C.; Hu, C.; Shen, W.; Wang, S.; Tian, Y.; Wang, X. Synthesis and characterization of $TiO_2$/CdS core–shell nanorod arrays and their photoelectrochemical property. *J. Alloys Compd.* **2012**, *523*, 139–145. [CrossRef]
27. Kim, M.R.; Kang, Y.-M.; Jang, D.-J. Synthesis and Characterization of Highly Luminescent CdS@ZnS Core−Shell Nanorods. *J. Phys. Chem. C* **2007**, *111*, 18507–18511. [CrossRef]
28. Chen, S.; Peng, Y.; Li, C.; Hou, Z. The co-decorated $TiO_2$ nanorod array photoanodes by CdS/CdSe to promote photoelectrochemical water splitting. *Int. J. Hydrogen Energy* **2021**, *46*, 32055–32068. [CrossRef]
29. Dang, W.; Xu, K.; Zhang, L.; Qian, Y. Fabrication of multilayer 1D $TiO_2$/CdS/ZnS with high photoelectrochemical performance and enhanced stability. *J. Alloys Compd.* **2021**, *886*, 161329. [CrossRef]

30. Revathi, M.; Jeyakumari, A.P. Fabrication of $TiO_2$/CdS heterostructure photoanodes and optimization of light scattering to improve the photovoltaic performance of dye-sensitized solar cells (DSSCs). *J. Mater. Sci. Mater. Electron.* **2021**, *32*, 11921–11930. [CrossRef]
31. Devaraji, P.; Gao, R.; Xiong, L.; Jia, X.; Huang, L.; Chen, W.; Liu, S.; Mao, L. Usage of natural leaf as a bio-template to inorganic leaf: Leaf structure black $TiO_2$/CdS heterostructure for efficient photocatalytic hydrogen evolution. *Int. J. Hydrogen Energy* **2021**, *46*, 14369–14383. [CrossRef]
32. Lu, Y.; Yi, G.; Zhou, H.; Liu, J.; Zhang, H.; Lu, L.; An, L. Arrays of needle-like $TiO_2$/CdS nanorod heterostructure photoelectrodes with enhanced photoelectrochemical properties fabricate by pulsed laser deposition. *Vacuum* **2021**, *184*, 109985. [CrossRef]
33. Yang, J.; Zeng, J.-H.; Yu, S.-H.; Yang, L.; Zhou, G.-e.; Qian, Y.-t. Formation Process of CdS Nanorods via Solvothermal Route. *Chem. Mater.* **2000**, *12*, 3259–3263. [CrossRef]
34. Ye, C.; Meng, G.; Wang, Y.; Jiang, Z.; Zhang, L. On the Growth of CdS Nanowires by the Evaporation of CdS Nanopowders. *J. Phys. Chem. B* **2002**, *106*, 10338–10341. [CrossRef]